nature portfolio

https://doi.org/10.1038/s41928-022-00713-1

Supplementary information

Bioinspired in-sensor visual adaptation for accurate perception

In the format provided by the authors and unedited

Bioinspired in-sensor visual adaptation for accurate perception

Fuyou Liao,[1,2] Zheng Zhou,[3] Beom Jin Kim,[4] Jiewei Chen,[1,2] Jingli Wang,[1,2,5] Tianqing Wan,[2] Yue Zhou,[2] Anh Tuan Hoang[4], Cong Wang,[1,2] Jinfeng Kang,[3] Jong-Hyun Ahn,[4,*] and Yang Chai[1,2,6]*

[1] *The Hong Kong Polytechnic University Shenzhen Research Institute, Shenzhen, China*
[2] *Department of Applied Physics, The Hong Kong Polytechnic University, Hong Kong, China*
[3] *Institute of Microelectronics, Peking University, Beijing, China*
[4] *School of Electrical and Electronic Engineering, Yonsei University, Seoul 03722, Republic of Korea*
[5] *Frontier Institute of Chip and System, Fudan University, Shanghai, China*
[6] *Research Institute of Intelligent Wearable Systems, The Hong Kong Polytechnic University, Hong Kong, China*

*Corresponding author. Email: ychai@polyu.edu.hk (Y. C.), ahnj@yonsei.ac.kr (J.-H. A.)

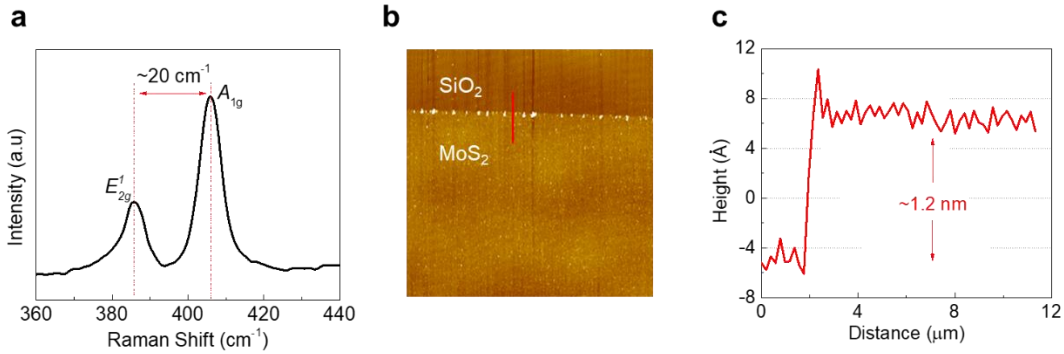

Figure S1. Thickness characterization of bilayer MoS_2. a, Raman spectrum of bilayer MoS_2 thin films using an excitation laser with a wavelength of 532 nm. The peak seperation between $E^1_{2g}$and A_{1g} (~20 cm^{-1}) confirms that the MOCVD MoS_2 is indeed a bilayer. **b, c,** The AFM topography image of the MoS_2 thin film and the corresponding height profile extracted from the red line. The thickness of the MoS_2 layer is ~1.2 nm, determined from the height profile, providing evidence for the bilayer MoS_2.

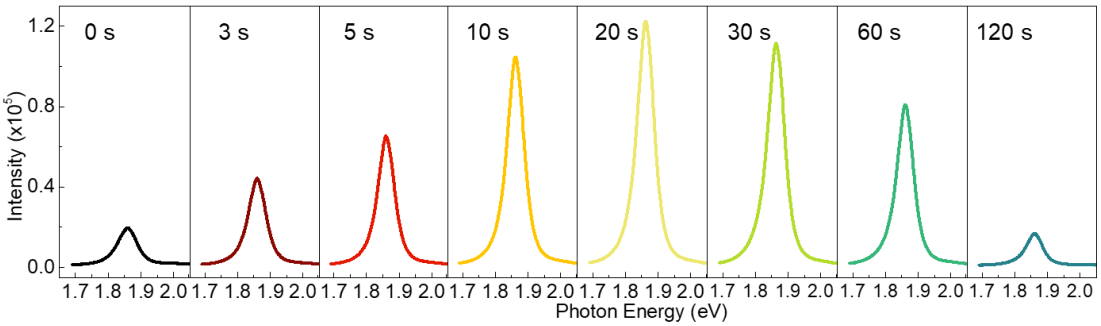

Figure S2. Photoluminescence spectra of bilayer MoS_2 with different UVO treatment duration from 0 to 120 s. The PL intensity at the peak of 1.86 eV increases with the UVO treatment duration from 0 to 20 s. The UVO treatment introduces more S vacancies in the MoS_2 layer, which are active centers for oxygen adsorption. These absorption sites give rise to conversion from trion to exciton emissions and suppress the nonradiative recombination of excitons at defect sites, which leads to the PL enhancement[1]. As the UVO treatment duration increase by more than 20 s, the formation of MoO_3, which is a wide bandgap semiconductor with an indirect bandgap, results in the decrease of PL intensity due to the non-radiative recomnation[2]. In this work, we aim to introduce more trapping centers without oxidizing the MoS_2 layer for visual adaptation functions. Therefore, we choose to treat the MoS_2 using relatively short-time UVO exposure (10 s) in this work. After finishing the UVO treatment, a 10-nm-thick Al_2O_3 was deposited on MoS_2 channel as an encapsulation layer.

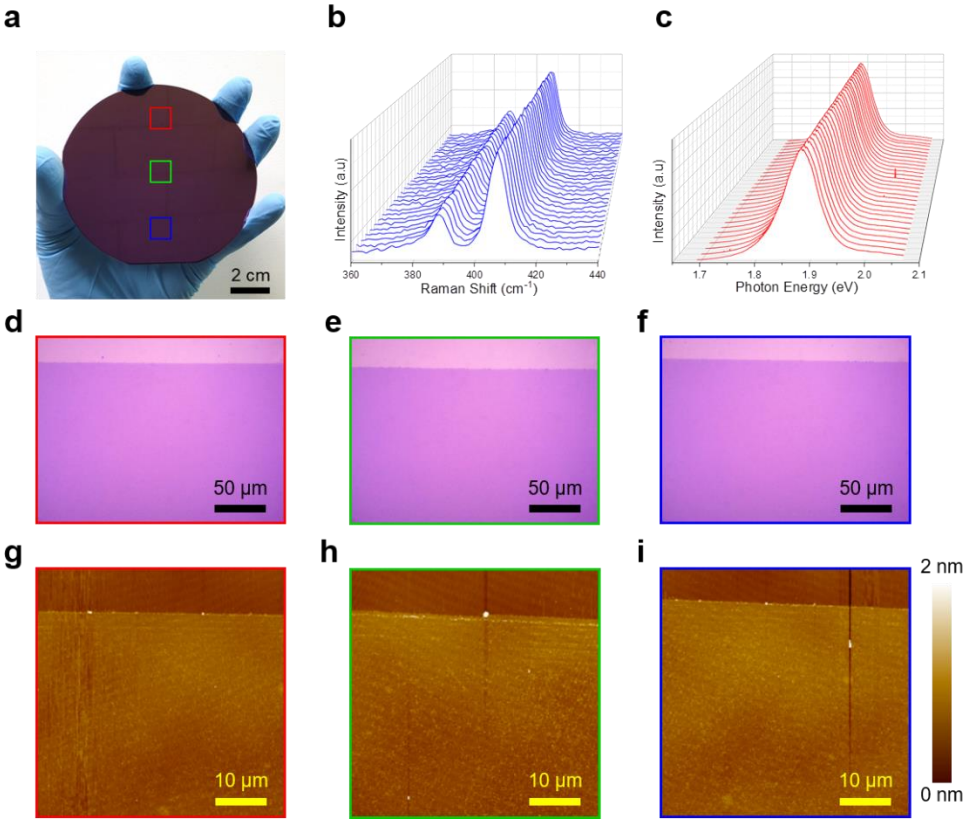

Figure S3. The uniformity of the large-scale MoS_2. a, Photograph of 4-inch wafer as-grown MoS_2. **b-c,** Raman and photoluminescence spectra of 30 points were measured randomly over the 4-inch wafer, respectively. There characteristics peaks of Raman and PL spectra are uniform without any peak shift. **d-f,** Optical microscope images of MoS_2 at the area marked in **a** and corresponding AFM topographic images showing in **g-i**. MoS_2 at marked areas present the same contrast with a smooth surface. The same thickness was confirmed by AFM measurement.

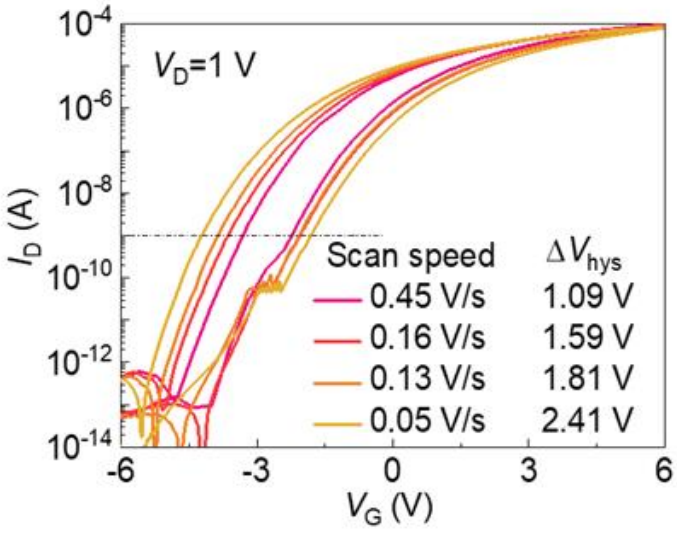

Figure S4. Transfer characteristic curves of a MoS_2 phototransistor at V_D=1 V under dark in an air atmosphere at different average scan speeds. The hysteresis windows (ΔV_{hys}) at a scan speed of 0.45, 0.16, 0.13, and 0.05 V/s are 1.09, 1.59, 1.81, and 2.41 V, respectively. The results illustrate that the slower scan rate has a larger ΔV_{hys}, because it allows more carriers to be trapped or de-trapped during the V_G sweep process. The calculated trap charge densities N_t are 1.09×10^{12}, 1.59×10^{12}, 1.81×10^{12}, and 2.41×10^{12} cm^{-2}, respectively.

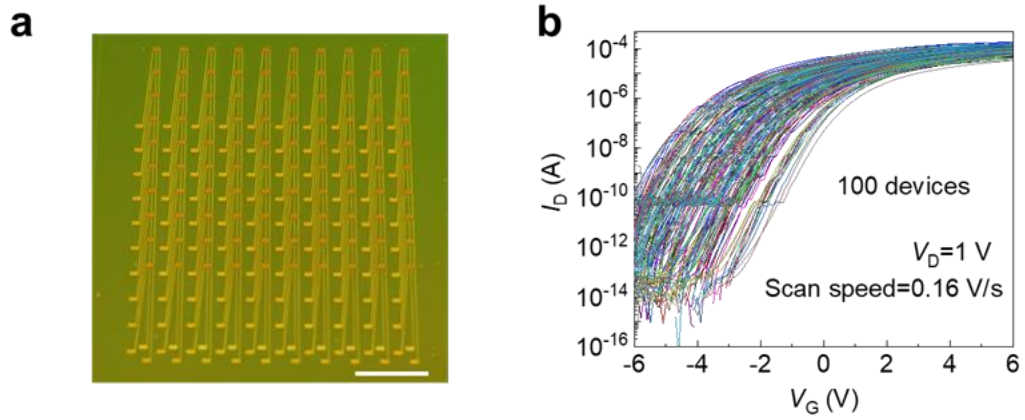

Figure S5. The electrical properties of the devices in the 10×10 array. a, A photograph of the as-fabricated MoS_2 phototransistor array on a diced 2.5×3.0 cm^2 chip. Scale bar: 4 mm. **b,** The typical transfer characteristics of 100 devices were measured with a scan speed of 0.16 V/s under dark conditions at V_D= 1 V.

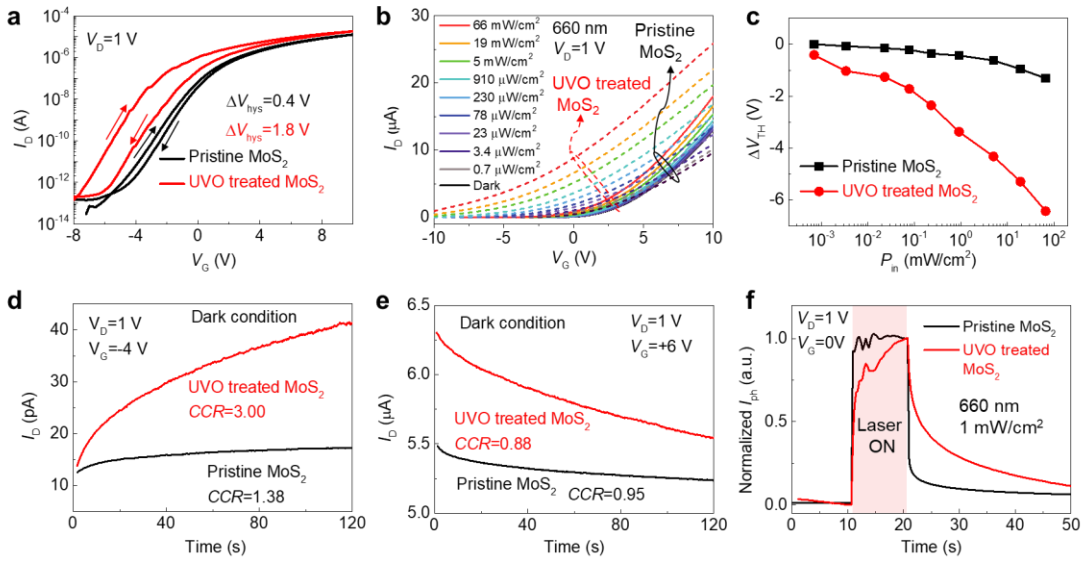

Figure S6. The characteristics of MoS_2 phototransistor before and after the UVO treatment with 63-nm-thick Al_2O_3 dielectric. a, The double-sweep transfer characteristic curves of a MoS_2 phototransistor before and after the UVO treatment at V_D=1 V under dark conditions at a scan speed of 0.4 V/s. The UVO treated MoS_2 transistor exhibits a larger hysteresis window (ΔV_{hys}=1.8 V) compared to the pristine MoS_2 phototransistor (ΔV_{hys}=0.4 V), suggesting that the UVO treatment can effectively introduce trap centers in MoS_2 transistor. **b,** Transfer characteristic curves of the MoS_2 device before and after the UVO treatment measured under different P_{in}. **c,** The extracted ΔV_{TH} of the MoS_2 phototransistor before and after the UVO treatment under different P_{in}. The ΔV_{TH} of the UVO treated MoS_2 phototransistor is more obvious than that of the pristine MoS_2 device under the same illumination condition, which further illustrates that the UVO treatment can introduce trap sates to the MoS_2 and enhance its photogating effect. Time-dependent I_D of the pristine and UVO treated MoS_2 phototransistor under dark conditions at V_G=-4 **d**, and **e**, +6 V, respectively. The current change ratio (*CCR*) of the pristine and UVO treated MoS_2 transistor at V_G=-4 V are 1.38 and 3.00, respectively; and the *CCR* of the pristine and UVO treated MoS_2 transistor at V_G=+6 V are 0.88 and 0.95, respectively. **f,** Normalized I_{ph} of the pristine and UVO treated MoS_2 phototransistor under the illumination of 1 mW/cm² for 10 s. The UVO treated MoS_2 phototransistors have a stronger persistent photoconductivity effect than that of the pristine MoS_2 phototransistor due to a large number of trap states in the MoS_2.

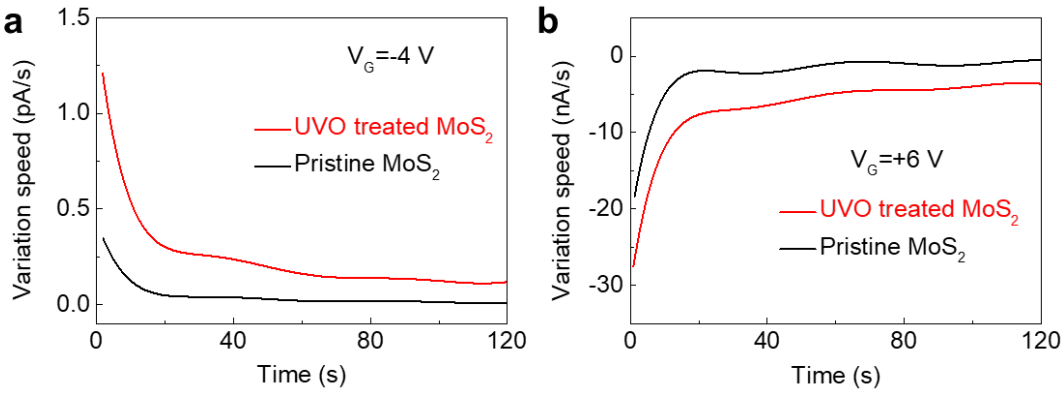

Figure S7. The current change speed of I_D in the pristine and UVO treated MoS_2 transistor extracted from Fig. S4 d and e. a, V_G=-4 V. **b,** V_G=+6 V. The current change speed of I_D in the UVO treated MoS_2 phototransistor is much faster than that of the pristine MoS_2 device, which demonstrates the UVO treated MoS_2 phototransistors have more obvious adaptation function and faster visual adaptation speed.

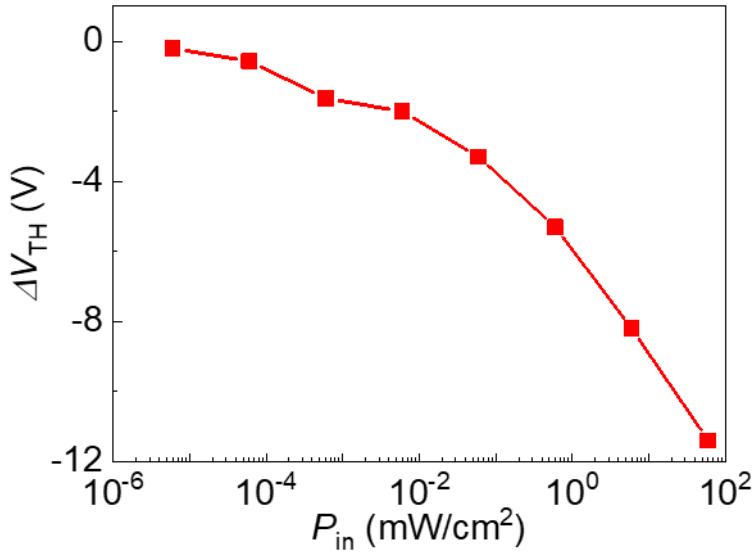

Figure S8. The extracted ΔV_{TH} of the UVO treated MoS_2 phototransistor under different P_{in}. $\Delta V_{TH}=V_{TH\text{-illumination}}-V_{TH\text{-dark}}$, where V_{TH} was calculated by fitting a straight line to the measured transfer curve.

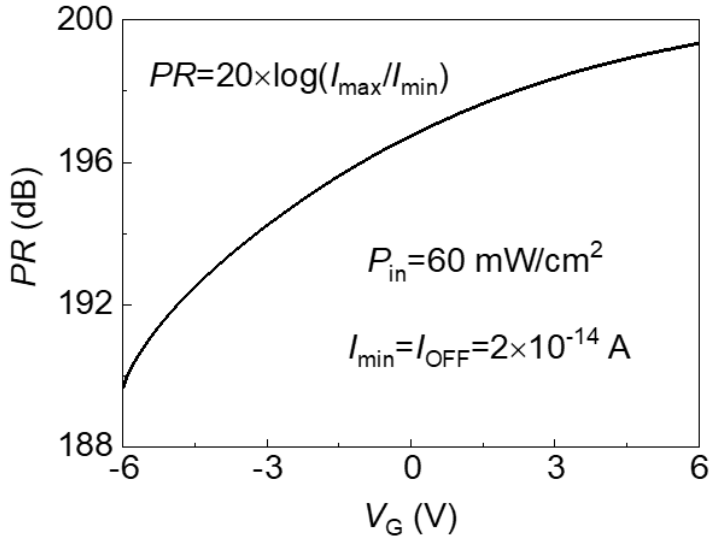

Figure S9. The effective perceived range dependent on V_G.

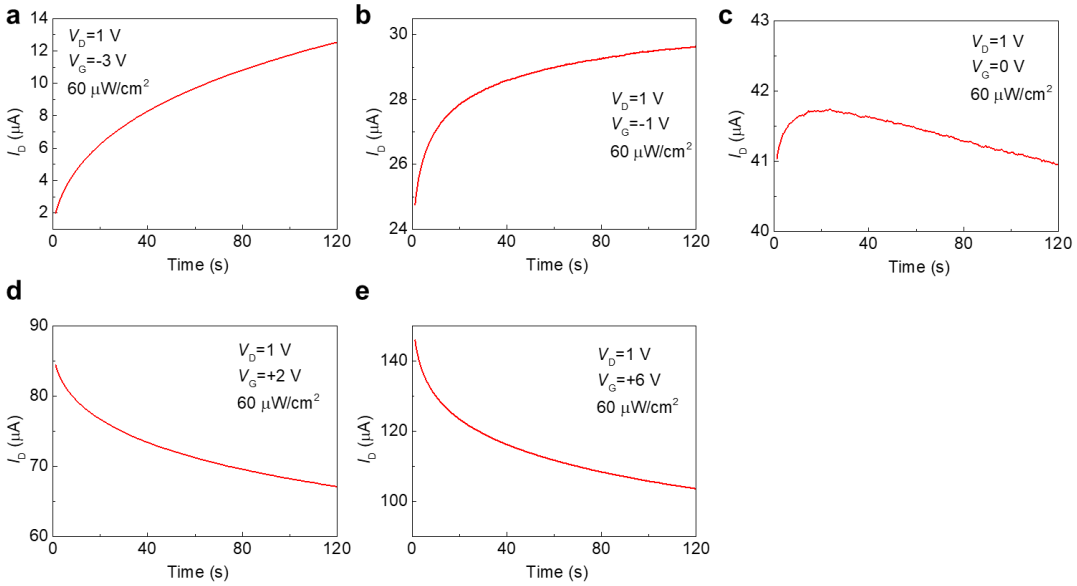

Figure S10. Current change of I_D of MoS_2 phototransistor over time under the illumination of 60 μW/cm^2 at different V_G. a, V_G=-3 V. **b,** V_G=-1 V. **c,** V_G=0 V. **d,** V_G=+2 V. **e,** V_G=+6 V.

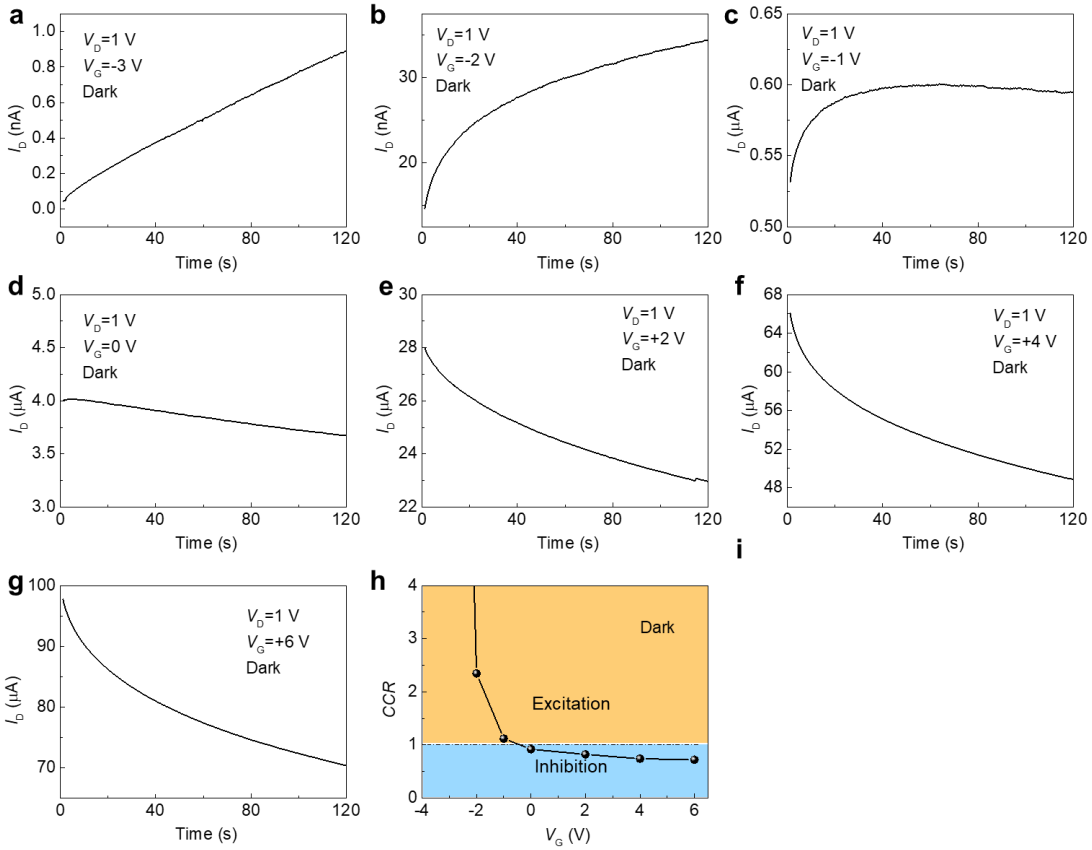

Figure S11. Current change of I_D of MoS_2 phototransistor over time under the dark condition at different V_G. a, V_G=-3 V. **b,** V_G=-2 V. **c,** V_G=-1 V. **d,** V_G=0 V. **e,** V_G=+2 V. **f,** V_G=+4 V. **g,** V_G=+6 V. **h,** The extracted *CCR* at different V_G.

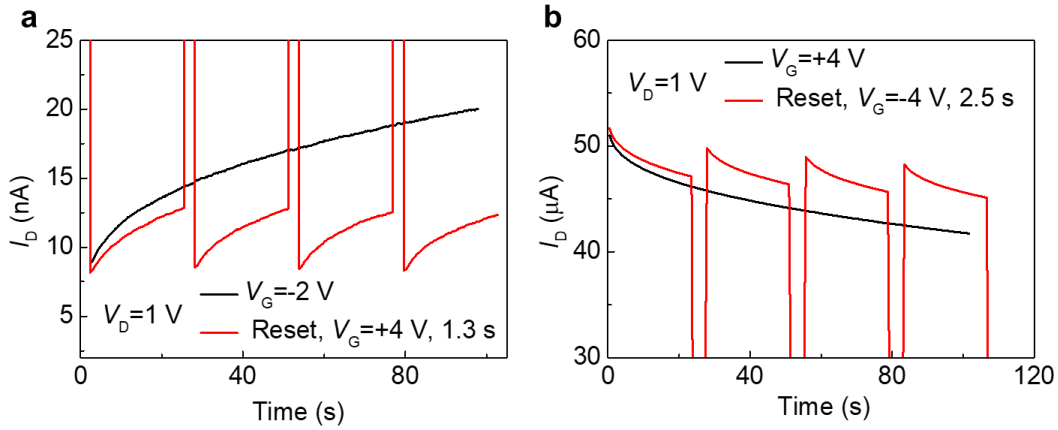

Figure S12. The electrically reset of the MoS_2 phototransistor. a, Current change of the I_D over time in the MoS_2 phototransistor at V_G=-2 V under dark conditions and reset by a positive V_G. **b,** Current of the I_D over time in the MoS_2 phototransistor at V_G=+4 V under dark conditions and reset by a negative V_G.

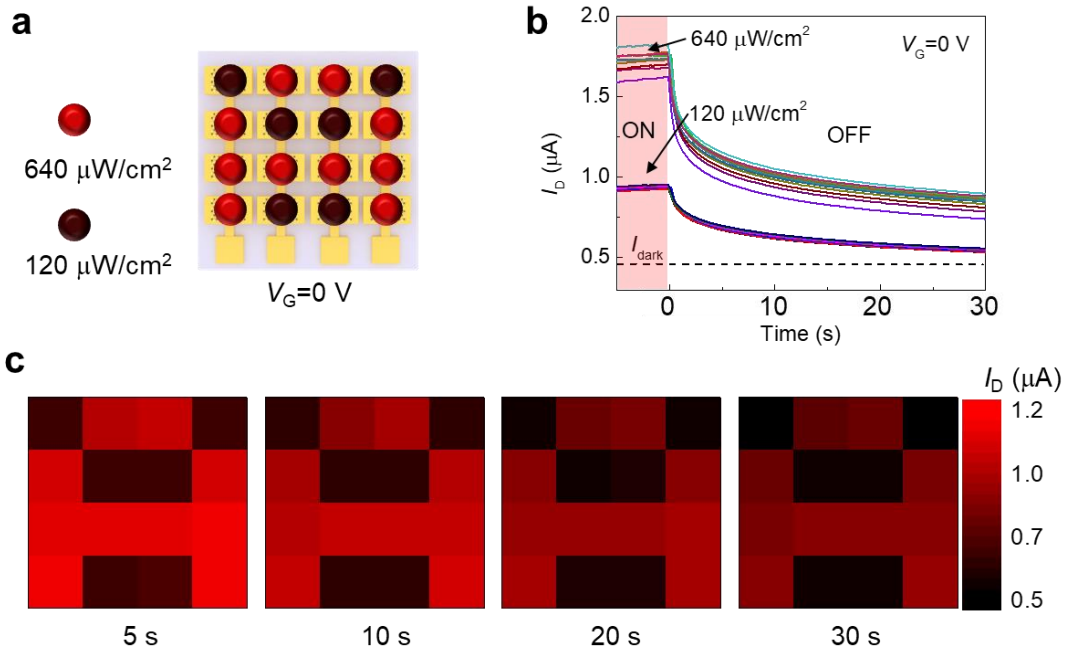

Figure S13. Image memorization of the MoS_2 phototransistors array with 63 nm Al_2O_3 dielectric. a, Schematic illustration of a 4×4 pixel array under a 120 μW/cm^2 background to recognize a 640 μW/cm^2 image for memorization test at V_G=0 V. **b,** Time-revolved photoresponse of 16 MoS_2 phototransistors after turning off the laser. **c,** Image memorization for a letter "*A*" pattern at 5, 10, 20, and 30 s after turning off the laser.

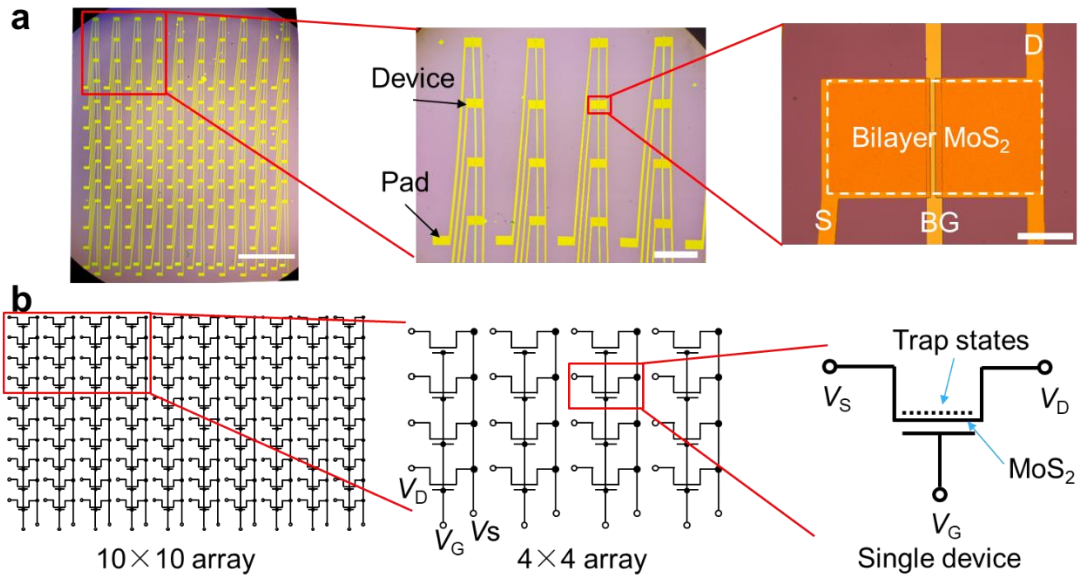

Figure S14. **The optical microscopy images of the 10×10 array a,** The equivalent circuits with different magnification. **b.** Scale bar: 4 mm (**a,** left). Scale bar: 1 mm (**a,** middle). Scale bar: 100 μm (**a,** right).

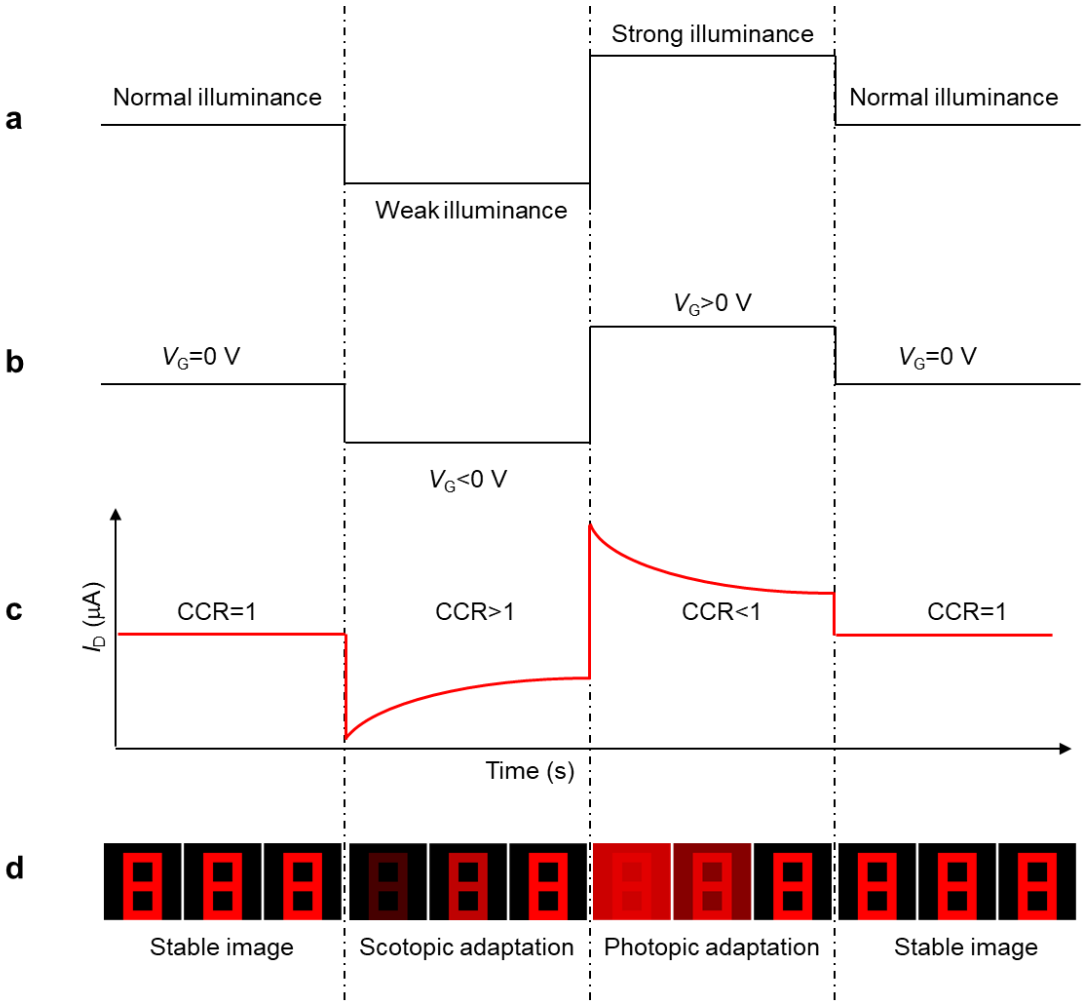

Figure S15. The schematic of measuring the bioinspired vision sensors for visual adaptation process according to the illuminance condition. **a,** The background illuminance condition. **b,** The applied V_G to vision sensor array. During the test, the V_G and the output voltage that controls the switch laser are switching simultaneously. **c,** Time-dependent current (I_D) of the device over time and its current change ratio (*CCR*). **d,** Image perception and its visual adaptation process.

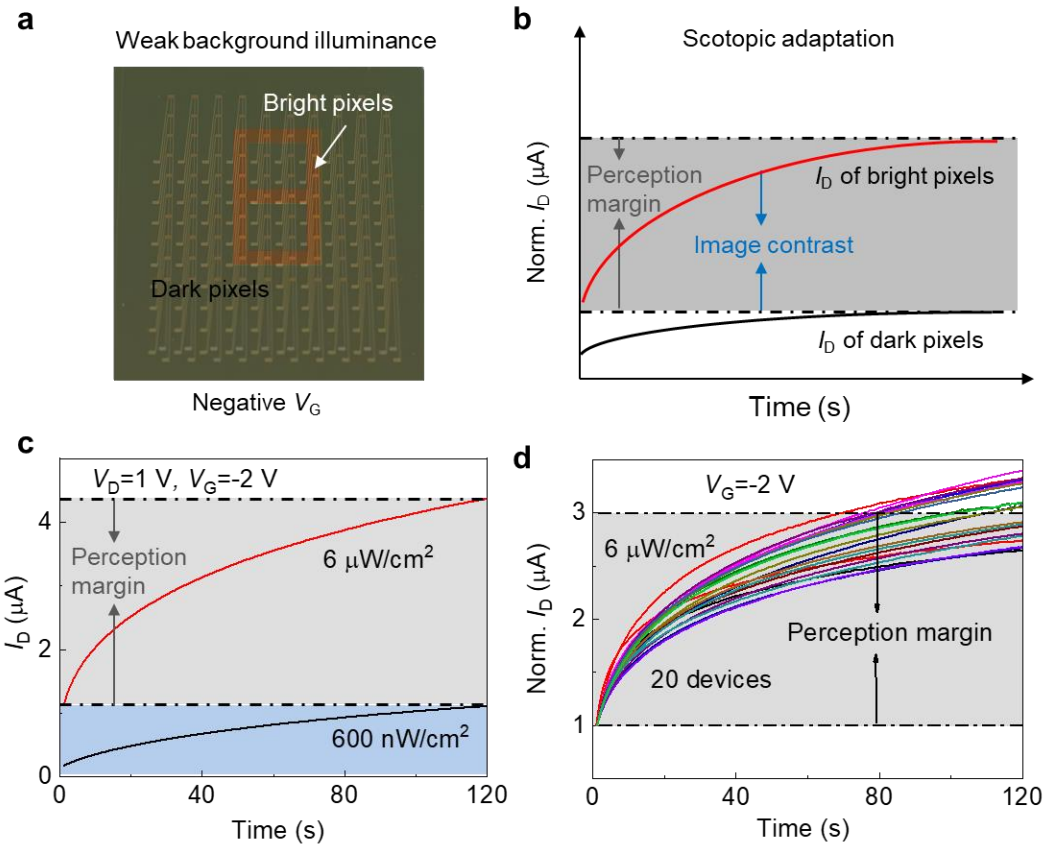

Figure S16. The schematic of measuring the bioinspired vision sensors for scotopic adaptation under a weak background illuminance. a, A devices array under a dark background to recognize a low-intensity pattern with negative V_G. The devices under low-intensity illumination are bright pixels, while the devices under dark background are dark pixels. **b,** The typical scotopic adaptation curves for the vision sensors. **c,** The time-dependent characteristics of a MoS_2 phototransistor under P_{in} of 6 μW/cm^2 and 600 nW/cm^2 at V_G=-2 V before normalized the I_D. **d,** Change of the normalized I_D in 20 devices (bright pixels) under P_{in} of 6 μW/cm^2 over time at V_G=-2 V.

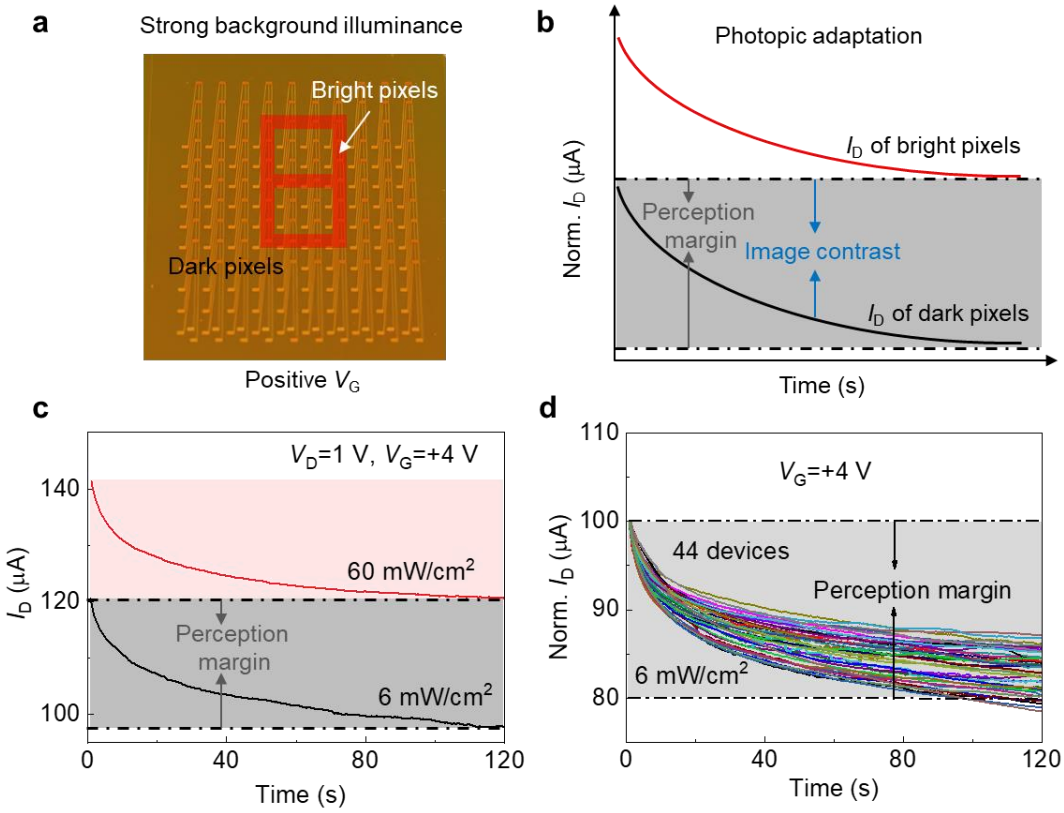

Figure S17. The schematic of measuring the bioinspired vision sensors for photopic adaptation under a strong background illuminance. a, A devices array under a bright background to recognize a high-intensity pattern with positive V_G. The devices under high-intensity illumination are bright pixels, while the devices under bright background are dark pixels. **b,** The typical photopic adaptation curves for the vision sensors. **c,** The time-dependent characteristics of a MoS_2 phototransistor under P_{in} of 60 mW/cm^2 and 6 mW/cm^2 at V_G=+4 V before normalized the I_D. **d,** Change of the normalized I_D in 44 devices (dark pixels) under P_{in} of 6 mW/cm^2 over time at V_G=+4 V.

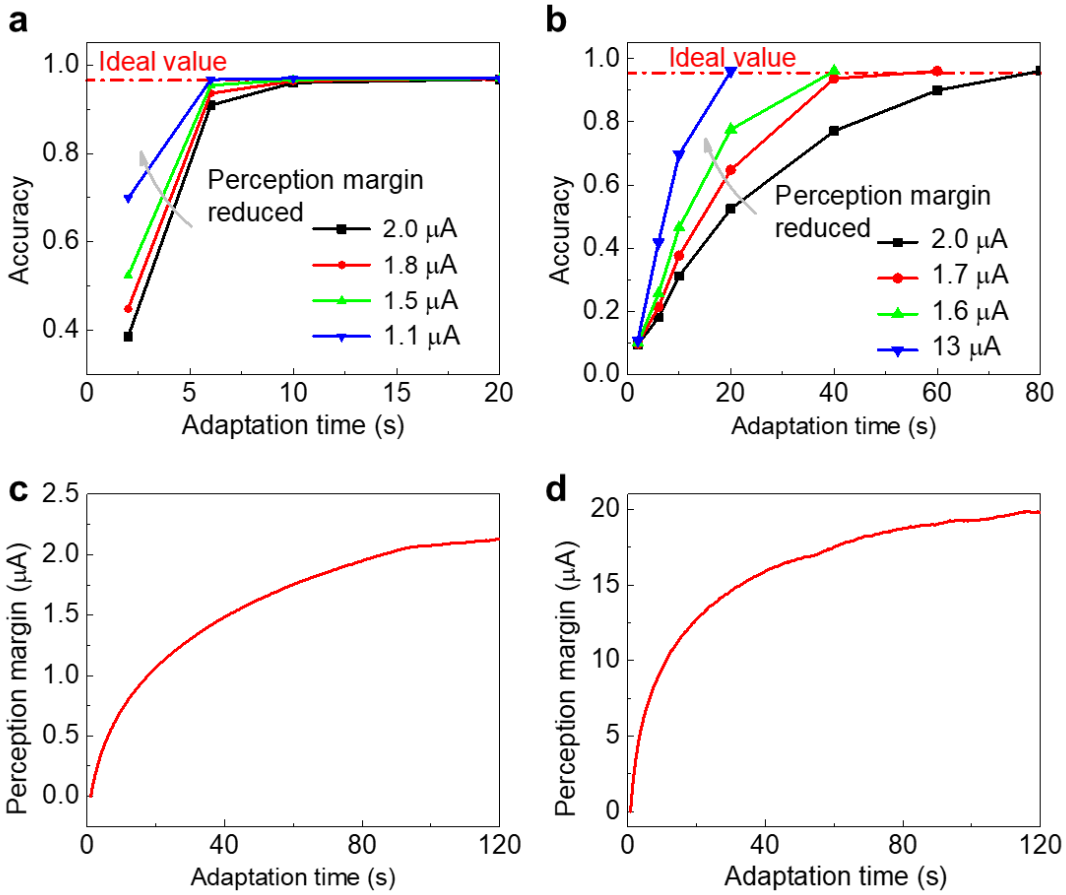

Figure S18. The impact of the perception margin on the adaptation time. The recognition rate as a function of time for the **a,** scotopic and **b,** photopic adaptation with different perception margins. The adaptation time as a function of perception margin at an ideal accuracy for the **c,** scotopic and **d,** photopic adaptation. **Fig. S15 a** and **b** show the relationship between the recognition accuracy and the adaptation time in the scotopic and photopic adaptation process. In both processes, the adaptation time needed to reach the ideal accuracy can be shortened by reducing the perception margin. The relationship between the adaptation time and the perception margin in scotopic and photopic adaptation processes are shown in **Fig. 15 c** and **d**. It means that a faster adaptation process needs more reliable device performance and more precisely peripheral circuit to distinguish grayscale in a narrower perception margin range.

The ANN follows the back propagation algorithm. The simulation process has two parts: 1) forming pattern recognition capability in a normal environment and 2)

recognizing patterns in different illumination environments. In the first part, the neural network is trained and tested by the MNIST dataset (handwriting digit number from '0' to '9', including 60000 training patterns and 10000 testing patterns) in a normal environment. The testing accuracy in this part verifies the recognition capability of the ANN, and can work as the baseline for the follow-up recognition tasks. In the second part, the testing pattern is exposed to a dim or bright environment. After the scotopic adaptation or the photopic adaptation in the MoS_2 phototransistor array, the modified patterns are recognized by the ANN. By comparing the recognition accuracy between the dim/bright environment and the normal environment, we can verify the pre-processing capacity of the adaptation in the MoS_2 phototransistor.

Table S1. The training and testing procedures of ANN.

Step	Dataset	Environment	Target	Algorithm
1	Training set	Normal	Training Network	Back propagation
2	Testing set	Normal	Accuracy Baseline	
3	Testing set	Dim	Scotopic Adaptation	
4	Testing set	Bright	Photopic Adaptation	

Table S2. Comparison of the proposed bioinspired in-sensor visual adaptation device with previous report.

Pixel structure	Visual adaptation	Scale	Adaptation time (s)	Perception range (dB)	Ref.
A MoS_2 phototransistor+ $CsPb(Br_{1-x}I_x)_3$ perovskite	Photopic adaptation	One pixel	>60	N/A	[3]
A MoS_2 phototransistor+ $CsPbBr_3$-Quantum-Dots	Photopic adaptation	One pixel	>4	N/A	[4]
A CsFAMA photovoltaic devices	Photopic adaptation	One pixel	4.8	N/A	[5]
An organic transistor that incorporates two bulk heterojunctions	Photopic adaptation	3×3	2	>120	[6]
A photovoltaic divider and an ionotronic synaptic transistor	Scotopic adaptation, Photopic adaptaton	3×3	10, 10	78	[7]
A MoS_2 phototransistor +UVO treatment	Scotopic adaptation, Photopic adaptaton	8×8	10, 80	199	This work

CsFAMA: Ternary cation halide $Cs_{0.05}FA_{0.81}MA_{0.14}PbI_{2.55}Br_{0.45}$

References

1 Nan, H. *et al.* Strong photoluminescence enhancement of MoS_2 through defect engineering and oxygen bonding. *ACS Nano* **8**, 5738-5745 (2014).

2 Kang, N., Paudel, H. P., Leuenberger, M. N., Tetard, L. & Khondaker, S. I. Photoluminescence Quenching in Single-Layer MoS_2 via Oxygen Plasma Treatment. *J. Phys. Chem.C* **118**, 21258-21263 (2014).

3 Hong, S. *et al.* Sensory Adaptation and Neuromorphic Phototransistors Based on $CsPb(Br_{1-x}I_x)_3$ Perovskite and MoS_2 Hybrid Structure. *ACS Nano* **14**, 9796-9806 (2020).

4 Xie, D. *et al.* Photoelectric Visual Adaptation Based on 0D-$CsPbBr_3$-Quantum-Dots/2D-MoS_2 Mixed-Dimensional Heterojunction Transistor. *Adv. Funct. Mater.* **31**,202010655 (2021).

5 Chen, Q. *et al.* Switchable Perovskite Photovoltaic Sensors for Bioinspired Adaptive Machine Vision. Adv. Intell. Syst. **2**, 2000122 (2020).

6 He, Z. *et al.* An organic transistor with light intensity-dependent active photoadaptation. *Nat. Electron.* **4**, 522-529 (2021).

7 Kwon, S. M. *et al.* Environment-Adaptable Artificial Visual Perception Behaviors Using a Light-Adjustable Optoelectronic Neuromorphic Device Array. *Adv. Mater.* **31**, 1906433 (2019).